

***Ab initio* molecular dynamics simulation of femtosecond laser-induced structural modification in vitreous silica**

S. Sen and J. E. Dickinson

Glass Research Divison, Corning Incorporated, Corning, New York 14831, USA

(Received 9 June 2003; published 24 December 2003)

Femtosecond laser pulse induced structural changes in silica glass and their role in changing the refractive index of the glass have been investigated using *ab initio* molecular dynamics simulation methods based on finite-temperature density functional theory. The average nearest-neighbor Si-O, Si-Si, and O-O distances are found to increase during laser irradiation due to the weakening of bonds resulting from the thermalization of electrons. These changes in the nearest-neighbor distances are almost completely recovered during the postirradiation evolution of the glass structure. However, persistent structural changes are found to involve the formation of three-coordinated Si atoms and nonbridging oxygens that correspond to the defect species of Si E' centers and nonbridging oxygen hole centers, respectively. These defects give rise to optical absorptions that increase the refractive index of silica glass through a Kramers-Kronig mechanism.

DOI: 10.1103/PhysRevB.68.214204

PACS number(s): 61.43.Fs, 61.43.Bn, 61.80.Ba, 71.15.Pd

I. INTRODUCTION

The interaction of infrared femtosecond laser pulses with dielectric solids, especially glasses, has received a great deal of research attention in recent years.¹⁻⁶ This is mainly because of the unique time scale of interaction of such ultrashort pulses with matter where the light energy is absorbed by the electrons and the excitation ends long before the energy is transferred to the lattice through electron-phonon interaction.^{7,8} Such ultrashort pulses have been used recently to change the refractive index of glass with high spatial precision thereby enabling the fabrication of waveguides without incurring any physical damage to the glass such as ablation or void formation.^{1,2} However, the actual mechanism controlling the change in the refractive index of the glass on interaction with femtosecond laser pulses remains unclear.²

A recent theoretical analysis by Kaiser *et al.* indicates that the principal effect of a femtosecond laser pulse is multiphoton ionization in the dielectric material associated with the strong electric field of a few hundred MV/cm of the laser pulse.⁷ Such ionization generates a free-electron gas by promoting a large number of electrons ($\sim 10^{18}$ to 10^{22} /cm³) from valence band into the conduction band of the dielectric material. The absorbed energy is then transferred to the lattice by electron-phonon collisions that result in the relaxation of the free-electron gas.⁷ A significant fraction of the absorbed photon energy is likely to get converted into heat which would then result in a rapid increase in the temperature of the lattice in the laser-exposed regions. Subsequent rapid cooling of these "hot spots" may give rise to regions of high fictive temperatures in the glass characterized by a refractive index that is different with respect to that of the surrounding unexposed regions. Moreover, as Glezer and Mazur have pointed out, a rapid rise in temperature within a constant volume element of exposed material may possibly be accompanied by a tremendous rise in pressure which would result in significant densification of the glass in the laser-exposed region.⁴ Such increases in fictive temperature

and/or pressure are expected to increase the refractive index of silica glass in femtosecond laser-exposed regions as has been observed experimentally in previous studies.^{2,3}

Recent studies have shown an increase in intensity of the D_1 and D_2 bands at ~ 490 and 605 cm⁻¹, respectively, in the Raman spectra of silica glass on irradiation of the glass with femtosecond laser pulses.^{2,3} This result has variously been interpreted in the literature to be indicative of an increase in the fictive temperature and/or densification of laser-irradiated silica glass and has been claimed to be responsible for the observed increase in refractive index.^{2,3} On the other hand, Streltsov and Borrelli have attempted calculations of the magnitude of rise in the temperature of the lattice of silica glass on the basis of the assumption that all the absorbed energy is converted into heat.² Their calculations indicate that the temperature rise of the lattice may not be enough to cause the observed increase in refractive index in silica glass especially when low pulse energies of a few nJ and high pulse repetition rates (~ 80 MHz) are used. Furthermore, calculations of index change from laser-induced densification as measured from stress-birefringence patterns indicate that densification alone cannot account for the observed index change in silica glass.² Therefore, these results make the connection between fictive temperature and/or pressure increase and index change rather arguable.

In view of this controversy we have carried out *ab initio* molecular dynamics (AIMD) simulations of the interaction of femtosecond laser pulses with silica glass to shed new light on the origin of the observed changes in the refractive index of the glass.

II. COMPUTATIONAL PROCEDURE

Our AIMD simulation methodology is based on finite-temperature density functional theory and follows the procedure outlined in the work of Silvestrelli *et al.* in their study of laser melting of crystalline silicon.⁹ This method treats the electronic and ionic subsystems separately on the basis of the fact that the electronic relaxation time is ~ 10 fs and is decoupled from the electron-ion relaxation time (\sim a few ps)

by nearly two orders of magnitude.⁹ The electronic subsystem in the simulation thermally equilibrates with the excess energy from the femtosecond laser pulse almost instantly and generates a free electron gas which is taken into account by increasing the electron temperature self-consistently with fractionally occupied states. The ions in the simulation are then allowed to interact with the hot electronic subsystem for 300 fs. In reality, however, the electron temperature is expected to continuously decrease from some maximum value at times longer than the laser pulse duration (\sim a few tens of fs) due to the relaxation of the hot free-electron gas through electron-phonon collisions.⁷ No attempt has been made in this study to simulate the details of the actual relaxation process of the hot free-electron gas through electron-phonon collisions. Instead the electron temperature is kept at its maximum value for times significantly longer (300 fs) than the pulse duration and the whole system is quenched instantaneously once the ions reach thermal equilibrium. The system of electrons and ions is then allowed to evolve without any further thermalization of the electrons to mimic the postirradiation evolution of the glass structure. Instantaneous quenching of the electrons after 300 fs rather than allowing it to equilibrate to the phonon bath is an extreme assumption. However, the essential physics of the mechanism of structure and index changes caused by femtosecond laser irradiation is not affected if one makes such an assumption in the simulation. This is because the specific heat of the phonon bath is much larger than that of the electron bath and therefore the temperature rise of the lattice on electron-phonon equilibration is not going to be large. Calculations of the rise in lattice temperature of vitreous silica for different experimental conditions by Streltsov and Borrelli have shown this to be the case.²

The starting structure of the silica glass was created from a 72 atom supercell of β quartz which was subsequently converted to a cubic cell with dimensions of 10.283 Å to yield a density of 2.20 g/cm³, appropriate for vitreous silica. This cell was melted and quenched using classical MD methods with two-body and three-body potentials provided by Feuston and Garofalini.¹⁰ The resultant glass was then annealed for 1 ps at 500 K using the *ab initio* method described below. AIMD simulations have been performed using the commercially available code DMol3 (Accelrys, Inc.) within an NVE ensemble with cubic periodic boundary conditions and with Γ -point-only sampling of the Brillouin zone. The DMol method is based on local orbital density functional theory and uses localized numeric atomic orbitals as basis sets.^{11,12} Double-numeric basis sets augmented with *d*-polarization functions are used for present simulations where all-electron calculations are performed within the local density approximation with the Harris functional approximation of the Kohn-Sham density functional.^{11,12} A real space basis set cutoff length of 4.5 Å is used. The forces on the ions are calculated using the Hellmann-Feynman theorem and the velocity Verlet algorithm is used to propagate the equation of motion. An integration time step of 0.5 fs is used for all dynamics simulations, with atom coordinates and velocities being saved after each time step. The instantaneous glass structure obtained at the end of each such time step is

saved for subsequent analyses.

Calculation of the absorption spectrum and refractive index for selected structures from the AIMD simulations were performed using the density functional theory code CASTEP in the local density approximation.¹³ Ultrasoft Vanderbilt pseudopotentials with a cutoff at 300 eV for Si and O were used to describe electron-ion interactions.¹⁴ For the initial evaluation of the self-consistent charge density a single-point energy calculation using a $2 \times 2 \times 2$ *k*-point mesh was performed.¹⁵ Following this, the evaluation of the optical matrix elements was initiated, also using a $2 \times 2 \times 2$ *k*-point mesh and allowing for twice as many unoccupied as occupied states. The optical matrix elements so calculated are used to evaluate the imaginary part of the dielectric constant, ϵ_2 , as a function of frequency ω , given by

$$\epsilon_2(\hbar\omega) = \frac{2e^2\pi}{\Omega\epsilon_0} \sum_{k,v,c} |\langle \Psi_k^c | \hat{\mathbf{u}} \cdot \mathbf{r} | \Psi_k^v \rangle|^2 \delta(E_k^c - E_k^v - E),$$

where the summation is over all *k* points and valence and conduction band states, Ω is the unit cell volume, and $\hat{\mathbf{u}}$ and \mathbf{r} are vectors defining the polarization of the incident electric field and the direction of propagation of light inside the material, respectively. The squared terms in brackets are the optical matrix elements. These arise due to coupling of the valence band states, Ψ_k^v , and the conduction band states, Ψ_k^c , via the operator $\hat{\mathbf{u}} \cdot \mathbf{r}$ describing the incident electric field. The last term simply describes the condition for absorption to occur between states in the valence and conduction bands with energies E_k^v and E_k^c , respectively. The real part of the dielectric constant ϵ_1 is then obtained by a Kramers-Kronig transformation from which the refractive index *n* as a function of frequency is obtained since $\epsilon_1 + i\epsilon_2 = n^2$. Finally, no attempt was made to adjust the calculated band gap to the experimental band gap using a scissor operator.¹⁶ While this certainly will impact the absolute value of the peak positions in the calculated absorption spectra and refractive index, the relative values, i.e., the values compared from different simulated structures, and which is of interest here, will be unaffected. A comparison of the calculated index of silica using the above methodology with the measured index is shown in Fig. 1. As expected, the calculated index is higher at all wavelengths compared to the experimental value, but what is most important here is that the wavelength dependence of the calculated index and measured index are the same. The similarity would be even more apparent if the calculated band gap had been adjusted using a scissor operator.

III. RESULTS AND DISCUSSION

To begin the simulation the electrons and ions in the cell are equilibrated for 1 ps by keeping the electron temperature T_{el} constant at 300 K by occupying the electronic levels according to the Fermi-Dirac statistics corresponding to this temperature. During this period the Si and O ions perform small oscillations around their equilibrium position and no change in the average glass structure is observed. The T_{el} is then raised to 25 000 K by occupying the electronic levels

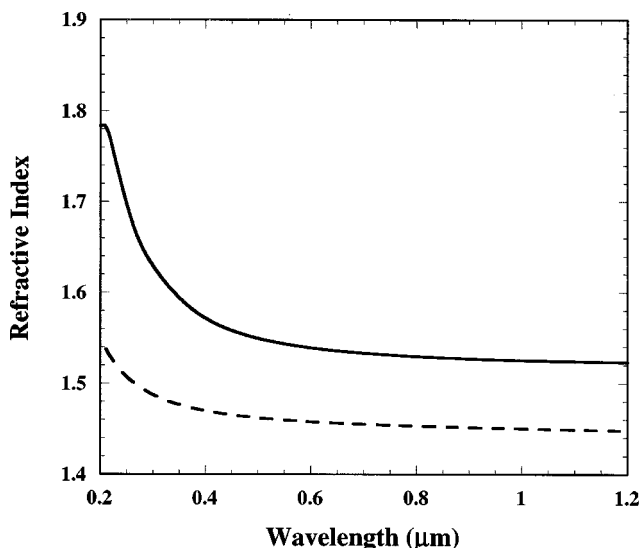


FIG. 1. Comparison of the measured (dashed line) and calculated (solid line) index of silica vs wavelength. No scissor operation has been applied to the calculated index.

accordingly, to simulate the effect of generation of the electron plasma on irradiation with femtosecond laser pulse. T_{el} of 25 000 K corresponds to a photon energy of 2.15 eV. This energy is intermediate between the energies typical of femtosecond laser amplifier (1.55 eV) and laser oscillator (3.09 eV) experiments.² The Si and O ions are then allowed to evolve freely for 300 fs within an NVE ensemble in the altered interatomic potentials defined by this new electron distribution. During this period the evolution of the average ion temperature T_{ion} as obtained from the kinetic energies of the Si and O ions is found to decrease from 300 K to ~ 280 K in the first 5 fs and then to increase monotonically to nearly 600 K in the next 30 fs (Fig. 2). At times longer than 30 fs T_{ion} undergoes a damped oscillation around 500 K and finally equilibrates to temperatures ~ 500 K at times longer than 250 fs. The observed oscillations in T_{ion} in our simulation are a direct result of instantaneous oscillations in the kinetic energy of the system. The running average of the

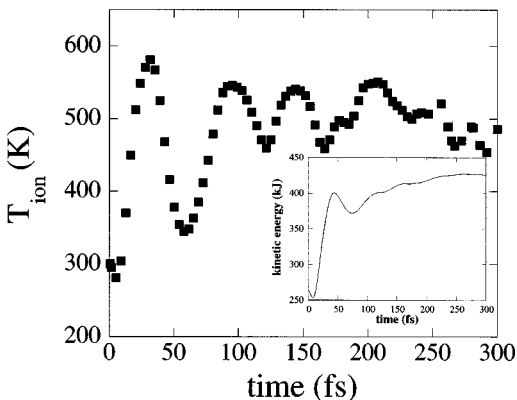


FIG. 2. Evolution of the instantaneous average temperature of Si and O ions in the simulation cell as a function of time at $T_{el} = 25000$ K. Inset shows the corresponding running average of the total kinetic energy of the ions.

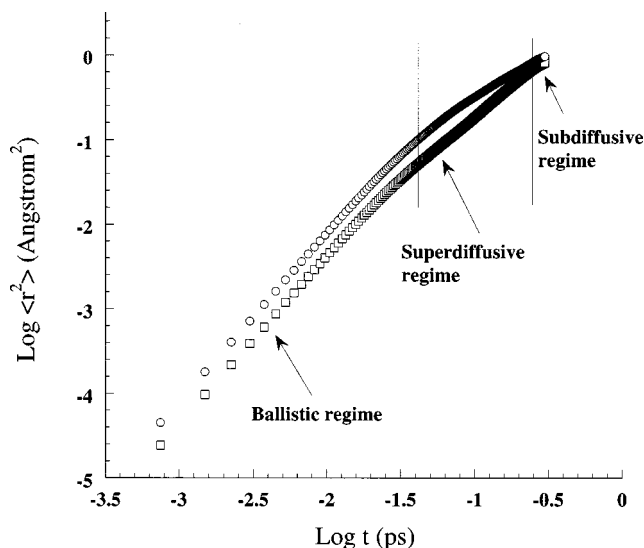


FIG. 3. Log-log plot of mean-squared displacements of Si (squares) and O (circles) atoms as a function of time at $T_{el} = 25000$ K. The two vertical lines separate the ballistic, superdiffusive, and subdiffusive regimes.

kinetic energy of ions shows convergence at times longer than ~ 250 fs indicating that the ions have approached thermal equilibrium with the electronic subsystem (Fig. 2). This equilibrium T_{ion} of ~ 500 K is substantially below both the melting point and the glass transition temperature of pure SiO_2 ($T_{melt} = 1983$ K, $T_g = 1480$ K). Nevertheless, the mean-squared displacements $\langle r^2 \rangle$ of Si and O atoms are found to be remarkably large over the entire 300 fs period of simulation (Fig. 3). Furthermore a log-log plot of $\langle r^2 \rangle$ vs time t indicates that in the initial ~ 40 fs the ionic motion is in fact ballistic with $\langle r^2 \rangle \sim t^2$ (Fig. 3). At times longer than ~ 40 fs the ionic motion continues to be superdiffusive with $\langle r^2 \rangle \sim t^x$ with $1 < x < 2$ and finally enters the subdiffusive regime ($x < 1$) at $t \geq 250$ fs. At $T_{el} = 25000$ K the cohesive force between ions is expected to decrease drastically since the bonding electrons are now excited to nonbonding levels. This may give rise to the ions drifting away from one other in an altered potential energy landscape which is in agreement with the observed initial ballistic motion of Si and O (Fig. 3). This scenario is clearly in contrast with that of laser-induced thermal “melting” which is expected to be associated with marked increase in the vibrational amplitude of ions. The continuous transition from the ballistic regime to the subdiffusive regime indicates that the ionic motion becomes increasingly localized with time as the ions start finding their equilibrium positions in the altered energy landscape. This result is consistent with the convergence of the running average of the kinetic energy of ions and the establishment of thermal equilibrium with the electronic subsystem at $t \geq 250$ fs, as mentioned above.

The total radial distribution function (RDF) for the starting structure of amorphous SiO_2 equilibrated at 300 K is compared in Fig. 4 with that obtained after 300 fs of the simulation run at $T_{el} = 25000$ K. This comparison shows that the average inter-ion distances of 1.62, 2.63, and 3.10 Å for the Si-O, O-O, and Si-Si nearest neighbors, respectively, in

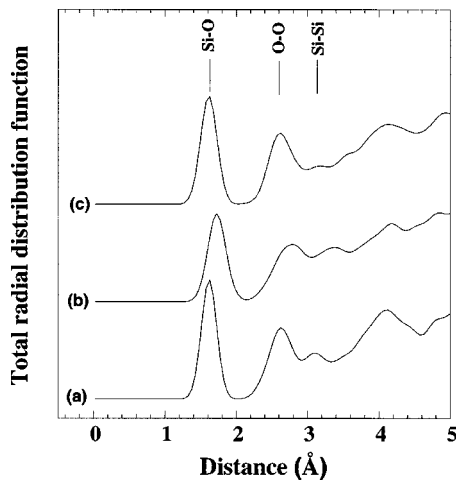


FIG. 4. Total RDF for (a) the starting structure, (b) the final structure of the 300 fs long “laser-exposure” simulation at $T_{el}=25000$ K, and (c) the final structure after 1 ps long “post-exposure” annealing at $T_{el}=300$ K. The positions of the nearest-neighbor Si-O, O-O, and Si-Si correlation peaks are also indicated.

the starting structure increase to 1.72, 2.77, and 3.34 Å in the structure corresponding to the irradiated glass. Such a large increase in the interion distances clearly indicates increasing repulsion between the constituent ions in the glass structure due to the change in the interatomic potential on generation of the electron plasma at high T_{el} . Moreover, the average Si-O nearest-neighbor coordination number is found to decrease from a value of 4.0 in the starting structure to ~ 3.8 in the irradiated glass as a result of the formation of some 3-coordinated Si atoms and concomitant formation of nonbridging oxygens. In fact, the structure of the irradiated glass (Fig. 5) shows four 3-coordinated Si atoms, six nonbridging oxygens, and one 2-coordinated Si atom.

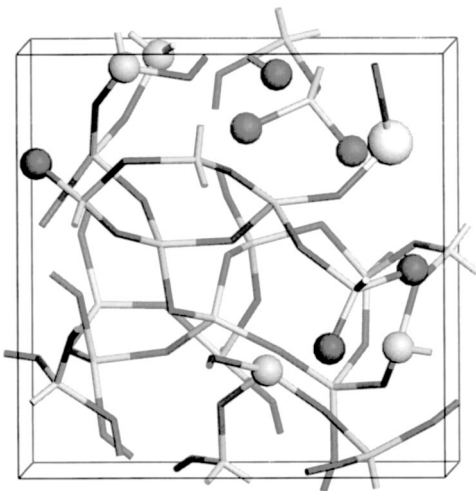


FIG. 5. Snapshot of glass structure after 300 fs at $T_{el} = 25000$ K. Dark spheres are non-bridging oxygens, lighter spheres are 3-coordinated silicons, and single large light sphere is a two-coordinated silicon.

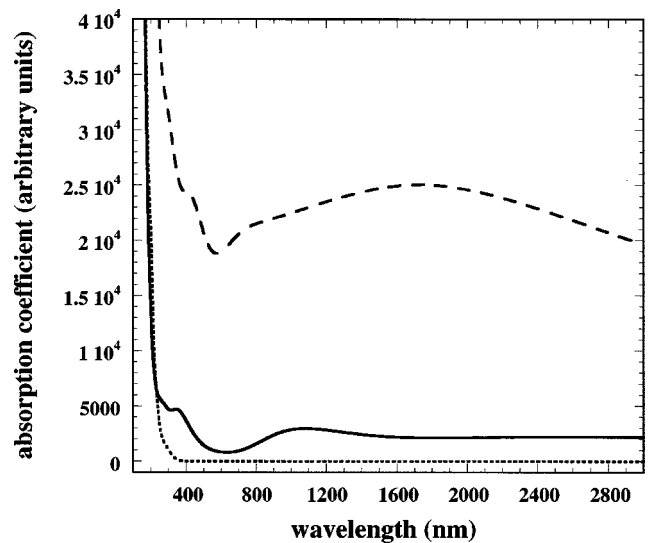


FIG. 6. Calculated optical absorption spectra of the starting structure (short-dashed line), “laser-irradiated” structure (long-dashed line), and “annealed” structure (solid line). Peaks in the spectra of the “exposed” and “annealed” structures correspond to electronic transitions involving NBOHC and E' defect centers.

Following the 300 fs long thermal equilibration between the ions and the electron plasma the postirradiation evolution of the glass structure has been simulated by lowering T_{el} back to 300 K and by continuing the AIMD simulation for 1 ps. The total RDF of the resulting glass structure is also shown in Fig. 4. It is clear that after this equilibration the average nearest neighbor distances are nearly completely restored to their original values. However, two 3-coordinated Si atoms and two nonbridging oxygens are found to survive in the final glass structure. Spatial separation of these underbonded Si atoms and nonbridging oxygens can give rise to charge separation and the creation of paramagnetic Si E' centers and nonbridging oxygen hole centers (NBOHC) in the glass. The Si E' centers have also been experimentally observed by Streltsov and Borrelli in fs-laser irradiated amorphous SiO_2 , using electron spin resonance (ESR) spectroscopy.² The calculated optical absorption spectra of the laser-irradiated and annealed structures show discrete absorption features at wavelengths less than about 500 nm or energies higher than ~ 2.5 eV and very broad features at wavelengths longer than 1000 nm or energies lower than ~ 1.25 eV (Fig. 6). The calculated electronic density-of-states (DOS) for the laser-irradiated and annealed structures as well as the partial DOS associated with the NBOHC and Si E' centers in these two structures are shown in Fig. 7. A comparison of the electronic DOS of these structures with that of the starting glass structure clearly indicates that the NBOHC and Si E' centers introduce discrete levels within the band gap of silica glass (Fig. 7). The energies associated with the transitions between these levels correspond well with the energies of the absorption features in the calculated optical absorption spectra, as mentioned above (Fig. 6).

The variation of the refractive index as a function of

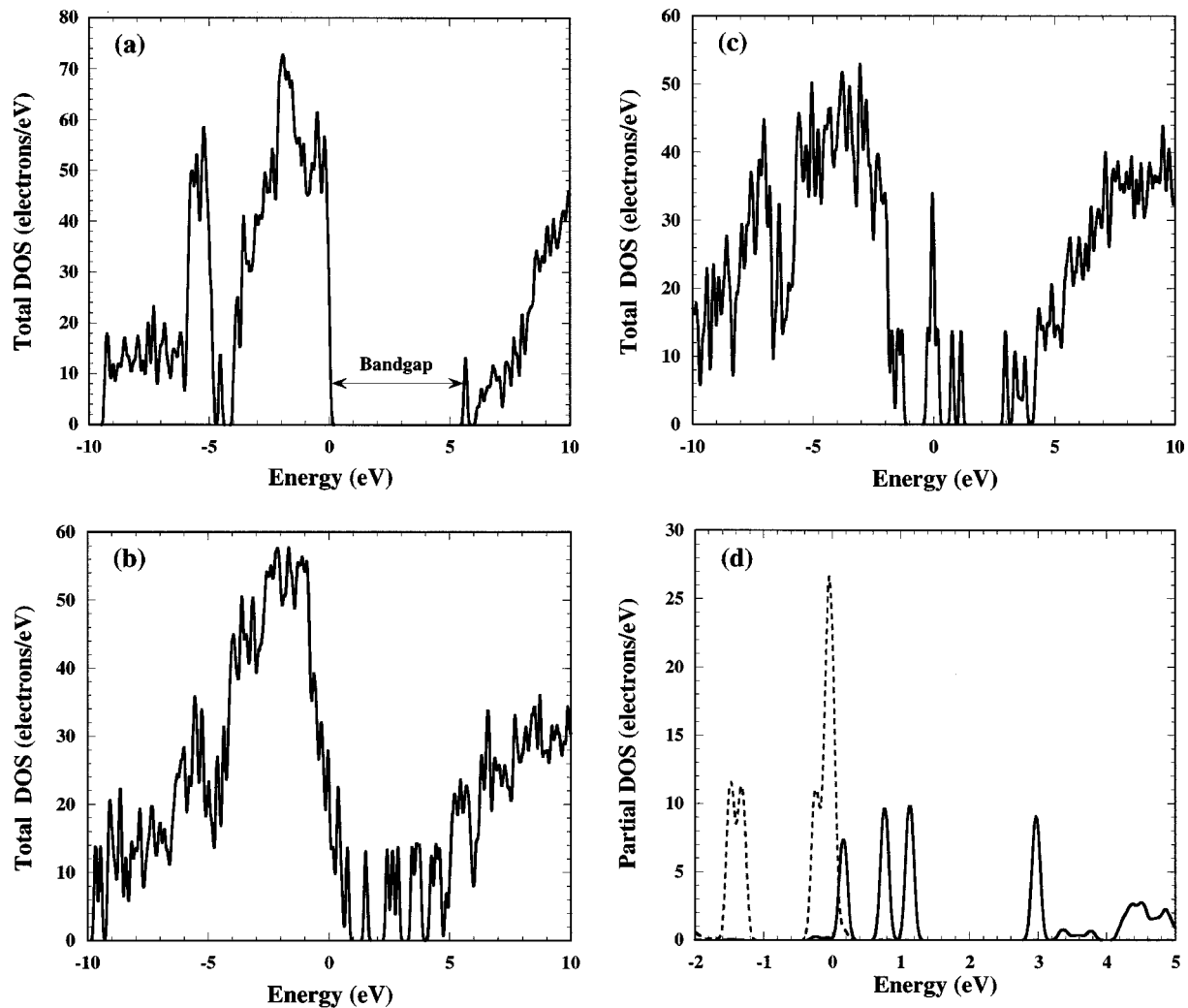


FIG. 7. Total electronic DOS for (a) the starting structure, (b) the “laser-irradiated” structure, (c) the “annealed” structure, and (d) partial electronic DOS for 3-coordinated Si (E' center) and nonbridging oxygens (solid and dashed lines, respectively) from the “annealed” structure. 0 eV marks the top of occupied levels. A 0.05 eV smearing function was used to broaden the energy levels.

wavelength as obtained from Kramer’s-Kronig analysis of the absorbance is shown in Fig. 8 for the starting structure, the structure obtained at the end of the 300 fs long simulation of “femtosecond pulse exposure” at $T_{el}=25000$ K and the final structure obtained after 1 ps of “post-exposure” annealing at $T_{el}=300$ K. It is quite apparent that the structural changes in the simulation have a strong effect on the resulting index. The indices at all wavelengths for the “laser-irradiated” structure and the “annealed” structure are significantly higher than the starting structure. The index variation in the short wavelength region below about 600 nm from the “laser-irradiated” and “annealed” structures are found to be due to the optical absorptions associated with the presence of NBOHC and E' center type of defects which perturb the index through a Kramers-Kronig mechanism. Higher concentration of such defects in the “laser-irradiated” structure is responsible for the larger change in index compared to that in the “annealed” structure. The continuous rise in index of the “laser-irradiated” structure at longer wavelength is also

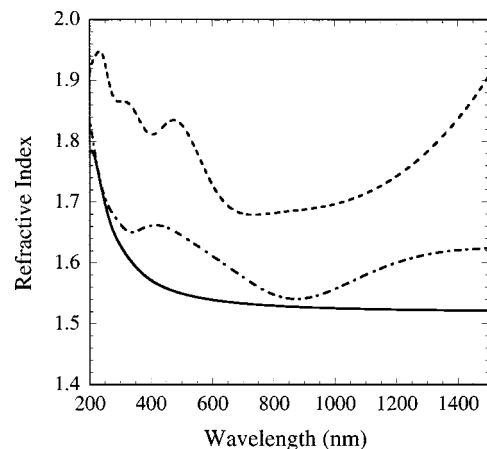


FIG. 8. Calculated wavelength dependence of the refractive indices of the starting structure (solid line), “laser-irradiated” structure (dashed line), and “annealed” structure (dot-dashed line). See text for details.

due to the presence of these defects in high concentration and the effect they have on narrowing the bandgap to only ~ 0.04 eV (Fig. 7). The practical implication of this index change during exposure is that the material becomes, effectively, totally absorbing to all wavelengths of radiation immediately after the exposure to the femtosecond laser pulse. This result is consistent with the experimental observation of the phenomenon of laser-induced breakdown of an initially transparent dielectric into a solid that absorbs like metal.⁷

IV. SUMMARY

In summary, structural origin of refractive index changes in silica glass caused by irradiation with femtosecond laser pulses has been investigated with AIMD simulation techniques. The most persistent laser-induced structural changes involve the formation of Si E' centers and NBO-HC's in the glass. Transitions between energy levels corresponding to these defects result in optical absorption that increase the index of the glass through a Kramers-Kronig mechanism.

¹K. Hirao and K. Miura, *J. Non-Cryst. Solids* **239**, 91 (1998).

²A. Streltsov and N. F. Borrelli, *J. Opt. Soc. Am. B* **19**, 2496 (2002).

³J. Chan, T. Huser, S. Risbud, and D. M. Krol, *Opt. Lett.* **26**, 1726 (2001); J. Chan, D. M. Krol, T. Huser, S. H. Risbud, and J. Hayden, *Glass & Optical Materials Division Fall Meeting Abstracts* (American Ceramic Society, Pittsburgh, PA, 2002).

⁴E. N. Glezer and E. Mazur, *Appl. Phys. Lett.* **71**, 882 (1997).

⁵K. Minoshima, A. M. Kowalevich, I. Hartl, E. P. Ippen, and J. G. Fujimoto, *Opt. Lett.* **26**, 1516 (2001).

⁶M. Lenzner, J. Krugler, S. Sartania, Z. Cheng, C. Spielmann, W. Kautek, and F. Krausz, *Phys. Rev. Lett.* **80**, 4076 (1998).

⁷A. Kaiser, B. Rethfeld, M. Vicanek, and G. Simon, *Phys. Rev. B* **61**, 11437 (2000).

⁸B. Rethfeld, A. Kaiser, M. Vicanek, and G. Simon, *Phys. Rev. B*

65, 214303 (2002).

⁹P. L. Silvestrelli, A. Alavi, M. Parrinello, and D. Frenkel, *Phys. Rev. Lett.* **77**, 3149 (1996).

¹⁰B. P. Feuston and S. H. Garofalini, *J. Chem. Phys.* **89**, 5818 (1988).

¹¹B. Delley, *J. Chem. Phys.* **113**, 7756 (2000).

¹²B. Delley, *J. Chem. Phys.* **92**, 508 (1990).

¹³V. Milman, B. Winkler, J. A. White, C. J. Pickard, M. C. Payne, E. V. Akhmatkaya, and R. H. Nobes, *Int. J. Quantum Chem.* **77**, 895 (2000).

¹⁴D. Vanderbilt, *Phys. Rev. B* **41**, 7892 (1990).

¹⁵H. J. Monkhorst and D. J. Pack, *Phys. Rev. B* **13**, 5188 (1976).

¹⁶R. W. Godby, M. Schluter, and L. J. Sham, *Phys. Rev. B* **37**, 10159 (1988).